Angular correlation analysis with Eurogam II

E.S. Paul

Oliver Lodge Laboratory, University of Liverpool, PO Box 147, Liverpool L69 3BX, UK

Abstract

Angular correlations $W(\theta_1, \theta_2, \Delta\phi)$ of cascade γ-rays emitted from oriented nuclear states are considered in relation to the Eurogam II multidetector spectrometer. General methods of analysis are discussed, including DCO analysis and complete angular correlation analysis.

September 1995

Contents

1 Introduction **2**

2 Definition of the angular correlation geometry **2**

3 Experimental analysis of angular correlation data **5**

4 Practical DCO analysis with Eurogam II **9**

5 Complete angular correlation analysis **10**

6 Extraction of experimental correlation intensities **11**

7 Results for the ^{31}P + ^{90}Zr reaction (EG43) **12**

7.1 Results for the individual geometries A–E 14

7.2 Results for the combined geometries A–E 17

8 Conclusions **18**

9 Acknowledgments **19**

1 Introduction

The measurement of angular correlations of coincident (cascade) γ-rays with multidetector arrays is a powerful tool for determining both the spin and parity (J^π) of excited nuclear states, together with the multipole mixing ratio (δ) of the emitted radiation. The use of $\gamma-\gamma$ coincidence data has the advantage over singles γ-ray angular-distribution measurements in that the γ-ray peaks are better separated in two dimensions with a lower background contamination. Historically, complete $\gamma - \gamma$ correlations from nuclear reactions (triple correlations) have been measured with NaI detectors [1, 2] and limited correlations (e.g. DCO[1] ratios [3, 4]) have been measured with high-resolution Ge detectors. The application of a complete $\gamma - \gamma$ correlation analysis to large γ-ray arrays has been addressed by Peter Ekström and coworkers [5], concentrating on the NORDBALL 20-detector spectrometer. The advent of the highly efficient "third generation" γ-ray multidetector spectrometers, such as EUROGAM, GAMMASPHERE, and GASP [6], offers the opportunity of extending the precise measurements of γ-ray angular correlations to ever weaker transitions. Thus, definite spin-parity assignments of nuclear states can be pushed to a much higher spin regime than previously possible. Moreover, a γ-ray "gated" angular correlation analysis is now feasible due to the increased statistics of $\gamma - \gamma - \gamma$ coincidence events obtained with the new spectrometers; such an analysis should further remove background contamination.

In this report, we consider an angular correlation analysis applied to the EUROGAM II spectrometer, using the codes developed in Ref. [5] to assess the method of analysis. Detailed theoretical aspects of γ-ray angular correlations can be found in Refs. [5, 7].

2 Definition of the angular correlation geometry

Following a heavy-ion fusion-evaporation reaction, the residual nuclei are aligned with their spin directions in a plane perpendicular to the beam axis (z-axis). The magnetic

[1]Directional Correlation from Oriented states

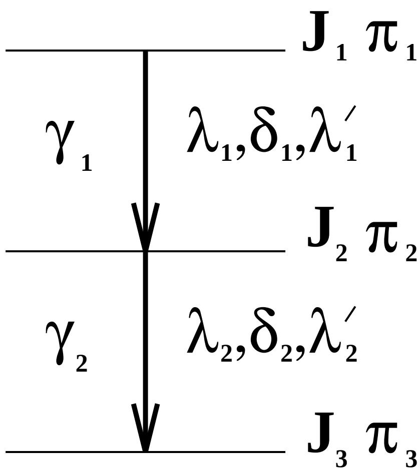

Figure 1: *Two γ-rays emitted in cascade from oriented states.*

substate population is usually assumed to form a Gaussian distribution about this "aligned" direction [5, 8]. Fig. 1 shows a cascade of two γ-rays depopulating such oriented states. The first γ-ray, γ_1, depopulates a nuclear state with spin J_1 and parity π_1, and feeds a state with spin J_2 and parity π_2. The lowest two multipolarities of the radiation are λ_1 and $\lambda_1' = \lambda_1 + 1$, with multipole mixing ratio δ_1. The possible multipolarities are restricted by

$$|J_1 - J_2| \leq \lambda_1, \lambda_1' \leq J_1 + J_2, \tag{1}$$

while the mixing ratio[2], δ_1, is related to the relative probabilities of the multipolarities (λ,λ') by

$$\delta_1^2 = \frac{T(\lambda_1')}{T(\lambda_1)}. \tag{2}$$

Since the parity change ($\pi_2 - \pi_1$) is fixed, the possible multipolarities are restricted to the two following sequences,

$$\begin{aligned} &E0, M1, E2, M3 \ldots \quad \text{for } \pi_1 = \pi_2, \qquad (3)\\ &E1, M2, E3, M4 \ldots \quad \text{for } \pi_1 \neq \pi_2, \end{aligned}$$

provided equation (1) is satisfied (note: $E0$ transitions are not allowed for $J_1 = J_2 = 0$, $M0$ transitions are also forbidden). Given that the transition probabilities rapidly decrease as

[2]theorists often use a "reduced" mixing ratio in which the energy dependence of equation (2) is removed

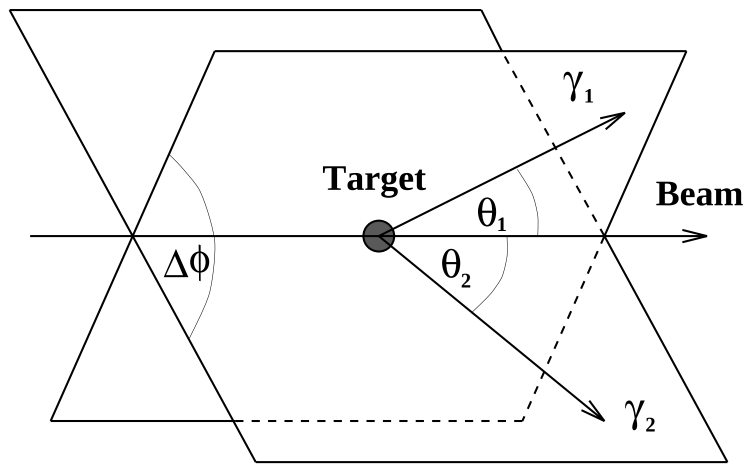

Figure 2: *Definition of the angles θ_1, θ_2, and $\Delta\phi$, for two γ-rays emitted in cascade from oriented states produced in a heavy-ion fusion-evaporation reaction.*

the multipole order increases, it is appropriate to consider only the two lowest multipole orders. Furthermore, since electric transitions of a given multipole order are more probable than magnetic transitions of the same order, it is only necessary to consider the competition of magnetic λ multipoles with electric λ' $(= \lambda + 1)$ multipoles. For example, it is adequate to consider only $E2/M1$ mixtures for most applications. Typical values for δ^2 $(E2/M1)$ are a few percent. Note, however, that δ itself may be related to a ratio of reduced matrix elements and therefore may be positive or negative [7], i.e. the *sign* of δ is physically meaningful. Different sign conventions have been used in the literature [8, 9]. In this report we adopt the sign convention of Ref. [8]. A similar notation is adopted for the second γ-ray, γ_2, in Fig. 1.

As depicted in Fig. 2, the two γ-rays are emitted (detected) at angles θ_1 and θ_2 with respect to the beam axis (z-axis), and the angle $\Delta\phi = \phi_1 - \phi_2$ is the angle between the planes defined by the z-axis and the outgoing γ-rays. The probability (intensity) for this specific configuration is given by the angular-correlation function [7]

$$W(\theta_1, \theta_2, \Delta\phi). \tag{4}$$

The multidetector EUROGAM II spectrometer [6] contains 54 Ge detectors at the angles (θ, ϕ) listed in Table 1. Thirty coaxial detectors are positioned in two rings of 5 and 10 detectors, respectively, at forward angles, and two corresponding rings of 5 and 10 detectors, respectively, at backward angles. Twenty four (four element) segmented clover detectors are positioned in two rings of 12 detectors near $\theta = 90°$. The 54 detectors of EUROGAM II constitute $(54\times53/2) = 1431$ detector pairs. However, due to symmetries of the angular-correlation function $W(\theta_1, \theta_2, \Delta\phi)$, reproduced below from Ref. [5],

$$W(\theta_1, \theta_2, \Delta\phi) = W(180° - \theta_1, 180° - \theta_2, \Delta\phi), \tag{5}$$

$$\begin{aligned} W(\theta_1, \theta_2, \Delta\phi) &= W(\theta_1, 180° - \theta_2, \Delta\phi + 180°) \\ &= W(180° - \theta_1, \theta_2, \Delta\phi + 180°), \end{aligned} \tag{6}$$

$$\begin{aligned} W(\theta_1, \theta_2, \Delta\phi) &= W(\theta_1, 180° - \theta_2, 180° - \Delta\phi) \\ &= W(180° - \theta_1, \theta_2, 180° - \Delta\phi), \end{aligned} \tag{7}$$

this number of detector pairs can be reduced to 83 equivalent pairs $(\theta_1, \theta_2, \Delta\phi)$, called "geometries", with $0° \leq \theta \leq 90°$ and $0° \leq \Delta\phi \leq 180°$. Table 2 shows the number of specific geometries for the EUROGAM II spectrometer, as calculated with the program COMBIN [5]. The segmented clover detectors are treated here as single detectors at an average position (θ, ϕ). Fourteen of the 83 geometries of EUROGAM II contain 40 or more detector pairs, as listed in Table 3 (arbitrarily labelled as geometries A–N), and hence provide sufficient statistics to assess the angular correlations $W(\theta_1,\ \theta_2,\ \Delta\phi)$ for a specific geometry.

3 Experimental analysis of angular correlation data

An experimental DCO ratio is often defined as

$$R_{\text{DCO}} = \frac{W(\theta_1, \theta_2, \Delta\phi = all)}{W(\theta_2, \theta_1, \Delta\phi = all)} \equiv \frac{I_{\gamma\gamma}(\theta_1, \theta_2[gate])}{I_{\gamma\gamma}(\theta_2, \theta_1[gate])}, \tag{8}$$

where all detectors in rings at angles θ_1 and θ_2 ($\theta_1 \neq \theta_2$), with respect to the beam axis, are considered irrespective of their $\Delta\phi$ values. Typically, a single $E_{\gamma_1} - E_{\gamma_2}$ correlation matrix is constructed of γ-rays detected at θ_1 against γ-rays detected at θ_2, from which the coincidence intensities $I_{\gamma\gamma}(\theta_1, \theta_2)$ and $I_{\gamma\gamma}(\theta_2, \theta_1)$ are extracted. A drawback of this method is that the $R_{\rm DCO}$ ratio, as defined in equation (8), depends on the multipolarity of the gating transitions, i.e.

$$R_{\rm DCO}[\text{quadrupole} \Leftrightarrow \text{quadrupole}] = R_{\rm DCO}[\text{dipole} \Leftrightarrow \text{dipole}], \tag{9}$$

$$R_{\rm DCO}[\text{quadrupole} \Leftrightarrow \text{dipole}] = R_{\rm DCO}[\text{dipole} \Leftrightarrow \text{quadrupole}], \tag{10}$$

when the transitions are *pure* ($\delta_1 = \delta_2 = 0$) and *stretched* ($J_1 - J_2 = \lambda_1,\ J_2 - J_3 = \lambda_2$) in character. Equation (9) indicates that $R_{\rm DCO}[E2 \Leftrightarrow E2] = R_{\rm DCO}[E1 \Leftrightarrow E1]$, and so care must be taken in choosing the gating transitions.

The ambiguity of the $R_{\rm DCO}$ ratio for quadrupole $\Leftrightarrow$ quadrupole and dipole $\Leftrightarrow$ dipole correlations may be removed by considering the ratio

$$R_{\rm DCO} = \frac{W(\theta_1, \theta_1, \Delta\phi = all)}{W(\theta_2, \theta_1, \Delta\phi = all)} \equiv \frac{I_{\gamma\gamma}(\theta_1, \theta_1[gate])}{I_{\gamma\gamma}(\theta_2, \theta_1[gate])}, \tag{11}$$

i.e. when the gating γ-ray is always detected at an angle θ_1, the ratio is *independent* of its multipolarity. This method requires the construction of two $E_\gamma - E_\gamma$ matrices, corresponding to θ_1 vs. θ_1 and θ_2 vs. θ_1, from which the coincident γ-ray intensities are extracted to form the $R_{\rm DCO}$ ratio. A further extension is to allow the second (gating) γ-ray to take on all values, and the DCO ratio becomes

$$R_{\rm DCO} = \frac{W(\theta_1, \theta = all, \Delta\phi = all)}{W(\theta_2, \theta = all, \Delta\phi = all)} \equiv \frac{I_{\gamma\gamma}(\theta_1, \theta[gate])}{I_{\gamma\gamma}(\theta_2, \theta[gate])}. \tag{12}$$

Again this method requires the construction of two $E_\gamma - E_\gamma$ matrices, corresponding to θ_1 vs. *all* and θ_2 vs. *all*, from which the intensities are extracted. The number of possible detector pairs in the two matrices may be different, a fact which must be taken into account when forming the ratios.

The DCO ratio for a pure stretched $M1$ transitions ($|J_2 - J_1| = 1,\ \delta_1 = 0$) is identical to that for an $E1$ transition (again pure and stretched), i.e.

$$R_{\text{DCO}}[\text{stretched } M1 \Leftrightarrow \text{stretched } E2] = R_{\text{DCO}}[\text{stretched } E1 \Leftrightarrow \text{stretched } E2]. \qquad (13)$$

However, if some mixing is present ($\delta_1 \neq 0$), the R_{DCO} value is perturbed depending on the sign of the multipole mixing ratio δ_1 ($E2/M1$). Positive values of δ_1 move the ratio *towards* (or even *beyond*) that for a stretched [$E2 \Leftrightarrow E2$] correlation (=1.0 for the ratio of equation (8)), while negative values of δ_1 move the ratio *further away* from the [$E2 \Leftrightarrow E2$] value. Hence the ratio for a mixed $M1/E2$ transition with a positive mixing ratio could look like a stretched [$E2 \Leftrightarrow E2$] correlation. A further ambiguity arises for *nonstretched* ($J_2 - J_1 = 0$) pure $E1$ (or $M1$) transitions, where

$$R_{\text{DCO}}[\text{nonstretched } E1 \Leftrightarrow \text{stretched } E2] \approx R_{\text{DCO}}[\text{stretched } E2 \Leftrightarrow \text{stretched } E2]. \qquad (14)$$

These ambiguities can be resolved by simultaneously measuring the linear polarisation of the γ-ray transitions, and can be achieved for the EUROGAM II spectrometer by using the segmented clover detectors as Compton polarimeters [11]. For instance, stretched $E2$ transitions and nonstretched $E1$ transitions have *opposite* polarisations.

For small detector arrays, these "averaging" methods of DCO analysis are necessary in order to improve the counting statistics. However, for the new generation of large arrays, with many highly efficient Ge detectors at various angles (θ, ϕ), vastly improved statistics can now be obtained for the individual geometries ($\theta_1,\ \theta_2,\ \Delta\phi$). For example, 7 distinct geometries containing 20 or more detector pairs are found for the NORDBALL spectrometer [5]. Hence 7 separate matrices (3 asymmetric plus 4 symmetric geometries) are sorted from which 10 independent correlation intensities $I_{\gamma\gamma}(\theta_1,\ \theta_2,\ \Delta\phi)$ can be extracted to be compared to theory. The advantage of using the complete angular correlations instead of the DCO ratios lies in a better accuracy of calculated multipole mixing ratios, as a result of the higher number of degrees of freedom in the fit of the theoretical angular-correlation function to the experimental data.

In the case of the EUROGAM II spectrometer, there are 9 geometries (A–I) containing 40 coaxial-detector pairs, and 5 geometries (J–N) containing 48 clover-detector pairs, as listed in Table 3. Five of the geometries (A–E) are asymmetric with $\theta_1 \neq \theta_2$ (R_{DCO} is physically meaningful), while nine geometries (F–N) are symmetric since $\theta_1 = \theta_2$ ($R_{\mathrm{DCO}} = 1.0$). Table 4 lists the detector pairs, at array positions (x,y), that constitute the A geometry[3] of EUROGAM II with angles $\theta_1 = 22.4°$, $\theta_2 = 46.4°$, $\Delta\phi = 18.0°$. Hence, in order to extract the correlation intensity $I_{\gamma\gamma}(22.4°, 46.4°, 18.0°)$, the 40 detector pairs of geometry A would have to be sorted into a single $E_x - E_y$ coincidence matrix (note that the $I_{\gamma\gamma}(46.4°, 22.4°, 18.0°)$ correlation intensity can also be extracted from this asymmetric matrix). Similarly, other matrices would have to be sorted; one matrix is needed for each geometry under consideration. Precise DCO ratios,

$$R_{\mathrm{DCO}} = \frac{W(\theta_1, \theta_2, \Delta\phi)}{W(\theta_2, \theta_1, \Delta\phi)} \equiv \frac{I_{\gamma\gamma}(\theta_1, \theta_2[gate], \Delta\phi)}{I_{\gamma\gamma}(\theta_2, \theta_1[gate], \Delta\phi)}, \tag{15}$$

can also be extracted from each of the asymmetric matrices. The sorting of the subsets of the total EUROGAM II data may be rather complex to setup, but can be achieved by the use of a 2-D look-up table for each geometry. There is a FAZSORT[4] available to generate a 4k×4k matrix (radware format) corresponding to a specific geometry.

A further extension possible with the new generation of arrays, which have an average fold of 4–5 γ-rays per event, is to use one γ-ray as a gate before producing the angular-correlation matrices. The gating γ-ray is allowed in any (θ, ϕ) detector, which, due to the approximate isotropic distribution of the detectors over 4π, should not greatly effect the angular correlation of the remaining γ-rays. Care, however, has to be taken in unfolding the events into gated pairs before incrementing the angular-correlation matrix such that "spikes" do not appear [10]. A gated FAZSORT[5] is available to produce a gated angular-correlation matrix corresponding to a specific geometry.

[3] all 83 geometries are listed in the file /home/user/esp/DCO/combin/eg2dets.out
[4] /home/user/esp/sorting/fazsort/phase2/i117/acsort, with input files angfile, geomfile
[5] /home/user/esp/sorting/fazsort/phase2/i117/acsort_gated, with input files angfile, geomfile

4 Practical DCO analysis with EUROGAM II

The program CORREL[6] can be used to calculate the angular-correlation function $W(\theta_1, \theta_2, \Delta\phi)$ for two detectors located at positions (θ_1, ϕ_1) and (θ_2, ϕ_2). Table 5 shows values calculated for the asymmetric geometries A–E of the EUROGAM II spectrometer, while Table 6 shows values calculated for the symmetric geometries F–I. A meaningful R_{DCO} ratio can be defined for the asymmetric geometries, and values for stretched $E2 \Leftrightarrow E2$ (quadrupole $\Leftrightarrow$ quadrupole) and $E1 \Leftrightarrow E2$ (dipole $\Leftrightarrow$ quadrupole) correlations are included in Table 5. It can be seen from Table 5 that, although the $W(\theta_1, \theta_2, \Delta\phi)$ values change, albeit slowly, with $\Delta\phi$, the calculated DCO values depend very little on the value of $\Delta\phi$. Hence, for a DCO analysis, it would be possible to add all five of the geometries A–E while maintaining a well-defined ratio. The five geometries could be sorted into one matrix for which there are a total of 200 (5×40) detector pairs, thus increasing the statistics. This is, in fact, equivalent to sorting *any* of the coaxial 20 detectors at $\theta_1 = 46.4°$ against *any* of the coaxial 10 detectors at $\theta_2 = 22.4°$, for which there are again 200 (20×10) combinations!

The R_{DCO} ratio discriminates better for pure dipole $\Leftrightarrow$ quadrupole and quadrupole $\Leftrightarrow$ quadrupole correlations as the the angular difference $\Delta\theta = \theta_1 - \theta_2$ between the detectors increases. For the EUROGAM II spectrometer, the largest difference, $\Delta\theta = 53.1°$, occurs when considering the forward/backward rings of 5 coaxial detectors ($\theta_1 = 22.4°$) and the 12-detector clover rings ($\theta_2 = 75.5°$). The average DCO ratio calculated for a pure dipole $\Leftrightarrow$ quadrupole correlation is $R_{\text{DCO}} \approx 0.45$ when $\Delta\phi$ is allowed to vary (cf. Table 5). Hence, a matrix of clover detectors vs. forward/backward rings could be sorted from which to obtain the R_{DCO} values. There are a total of 240 (24×10) detector pairs available for this method; a FAZSORT[7] is available.

The two methods outlined above need only one angular-correlation matrix each. The drawback, however, as pointed out in the previous section, is that the extracted R_{DCO} ratio

[6] /usr/local/nsfbin/correl
[7] /home/user/esp/sorting/fazsort/phase2/i117/dcosort

depends on the multipolarity of the gating transition. This can be overcome by using ratios of the form shown in equations (11) and (12). Most statistics would be obtained for equation (12), and could be implemented by sorting matrices of *all* vs. forward/backward rings ($\theta_1 = 22.4°$) and *all* vs. clovers ($\theta_2 = 75.5°$). These two matrices contain 720 (24 clovers $\times$ the remaining 30 detectors) and 440 (10 coaxial detectors $\times$ the remaining 44 detectors) detector pairs, respectively. If detectors in the clover and forward/backward rings are also included on the *all* axis, these number of combinations rise to 996 (an extra $24{\times}23/2 = 276$ clover combinations) and 485 (an extra $10{\times}9/2 = 45$ coaxial combinations), respectively. The normalisation factors between the two matrices is given by the ratio of number of detector pairs ($440/720 = 0.611$ or $485/996 = 0.487$). The different efficiencies of the coaxial detectors ($\sim 70\%$) and clover detectors ($\sim 125\%$ in add-back mode) must also be considered. Strictly speaking, the different efficiency curves for *all* 54 detectors should be considered (see Section 6). This method of DCO analysis utilises the largest number of detector pairs and hence can be applied to the *weakest* structures of current interest, e.g. superdeformed (SD) bands. The quadrupole (E2) nature of SD transitions has been demonstrated in the mass 130 [12], mass 150 [13], and mass 190 [14] regions.

5 Complete angular correlation analysis

Whereas a DCO analysis is limited to the *asymmetric* geometries, a complete angular correlation analysis also utilises the *symmetric* geometries and is particularly advantageous for dipole transitions. For precise measurements of multipole mixing ratios, the experimental angular-correlations intensities $I_{\gamma\gamma}(\theta_1,\ \theta_2,\ \Delta\phi)$ can be compared to theory using the code GCORR [5]. Theoretical expressions (complex!) for the angular-correlation function $W(\theta_1,\ \theta_2,\ \Delta\phi)$ are given in Refs. [5, 7] and depend on

$$\theta_1, \theta_2, \Delta\phi, J_1, \pi_1, J_2, \pi_2, J_3, \pi_3, \lambda_1, \delta_1, \lambda_1', \lambda_2, \delta_2, \text{and } \lambda_2'. \tag{16}$$

Typically, one transition (e.g. γ_1) is allowed to be of mixed dipole character ($\delta_2 = 0$, δ_1 undefined) and the multipole mixing ratio δ_1 is treated as a free parameter. The value of δ_1 is determined by a χ^2 minimisation analysis. Note that γ_1 and γ_2 need not be *consecutive*, i.e. "nonobserved" intermediate γ-rays may be considered[8].

If the mixing ratio is consistent with zero, then the dipole transition is usually assumed (more-likely) to be electric rather than magnetic in nature (i.e. $M1/E2$ mixing is possible but not $E1/M2$). This assumption can be confirmed, or otherwise, by measuring the linear polarisation of the dipole transition.

6 Extraction of experimental correlation intensities

In order to compare the experimental $I_{\gamma\gamma}(\theta_1, \theta_2, \Delta\phi)$ intensities to the theoretical $W(\theta_1, \theta_2, \Delta\phi)$ probabilities, the experimental "number of counts" (or "volume" $V_{\gamma\gamma}(\theta_1, \theta_2, \Delta\phi)$) for the coincident pair $E_{\gamma_1} - E_{\gamma_2}$ must be determined, and corrected for the detection efficiency. The volume for the coincident pair $E_{\gamma_1} - E_{\gamma_2}$ may be obtained as the number of counts of γ_1 in a 1-D spectrum gated (projected out of a matrix) by γ_2. In constructing a DCO ratio, the intensities are often obtained from 1-D spectra gated by a sum of (quadrupole) transitions, i.e. the DCO ratios are averaged over several different γ-rays (γ_2).

Alternatively, the peak volume $V_{\gamma\gamma}(\theta_1, \theta_2, \Delta\phi)$ for a specific $E_{\gamma_1} - E_{\gamma_2}$ pair may be directly obtained from the angular-correlation matrix using the program XLII [17]. The matrix is usually background subtracted first, using the method of Ref. [18]; the package BAC-PAC[9] can be used to perform this subtraction. The program CORR_EFF [5] calculates correlation intensities, $I_{\gamma\gamma}(\theta_1, \theta_2, \Delta\phi)$, from the peak volumes taking into account the efficiency $\varepsilon_{\mathrm{X}}(E_{\gamma_1}, E_{\gamma_2})$ for detecting the $\gamma_1 - \gamma_2$ pair for geometry X, i.e.

$$I_{\gamma\gamma}(\theta_1, \theta_2, \Delta\phi) = \frac{V_{\gamma\gamma}(\theta_1, \theta_2, \Delta\phi)}{\varepsilon_{\mathrm{X}}(E_{\gamma_1}, E_{\gamma_2})}, \tag{17}$$

[8]Help on the input can be found in the source code /usr/local/nsfsrc/dco/gcorr/gcorr.f
[9]written by Mats Bergström

where the efficiency for detecting the pair of γ-rays for geometry X is given by

$$\varepsilon_{\mathrm{X}}(E_{\gamma_1}, E_{\gamma_2}) = \sum_{i,j,\in \mathrm{X}} \varepsilon_i(E_{\gamma_1}).\varepsilon_j(E_{\gamma_2}), \tag{18}$$

and the efficiency $\varepsilon(E_\gamma)$, is modelled by the function

$$\varepsilon(E_\gamma) = \exp\left(a + bx + cx^2 + dx^3 + ex^4 + fx^5\right), \tag{19}$$

where $x = \log\left(E_\gamma(keV)/1000\right)$. The 54 detectors of the Eurogam II spectrometer each require an efficiency curve of this form.

7 Results for the ^{31}P + ^{90}Zr reaction (EG43)

In October 1994, an experiment was undertaken with the Eurogam II spectrometer, at the Centre de Recherches Nucléaires, Strasbourg. The temperamental Vivitron electrostatic accelerator provided a "nominal" 150-MeV ^{31}P beam to bombard two stacked self-supporting foils of ^{90}Zr (>97% enriched), each of thickness 440 μg/cm^2. High-spin states in ^{117}I were populated via the strong 2p2n exit channel, while states in $^{116-118}$Xe were populated via pxn channels (x=2–4). Many other reaction channels, however, were also populated with significant strength, namely the $^{115,116,118}_{53}$I, $^{113-117}_{52}$Te, and $^{112-114}_{51}$Sb nuclides; i.e. this was a "messy" reaction! Approximately 8.5×10^8 high-fold γ^n coincidence events ($n\geq5$) were accumulated in 48 hours of beam time [15]. A partial decay scheme deduced for ^{117}I, using the Escl8r and Levit8r graphical analysis codes [16], is shown in Fig. 3.

An angular correlation analysis of this data set, using the methods outlined in this report, is currently underway. For simplicity, in the preliminary analysis, only the asymmetric coaxial-coaxial detector geometries A–E are considered, and the efficiency curves of the 30 coaxial detectors are assumed equal. For a single DCO matrix (e.g. geometries A–I containing only coaxial detectors), the efficiency factor (equation (18)) will then cancel in forming the R_{DCO} ratio. The validity of this assumption of equal efficiencies may be verified by comparing the intensities $I_{\gamma\gamma}(\theta_1, \theta_2, \Delta\phi)$ and $I_{\gamma\gamma}(\theta_2, \theta_1, \Delta\phi)$ extracted from the correlation matrices. For a symmetric geometry ($\theta_1 = \theta_2$), these intensities should always be

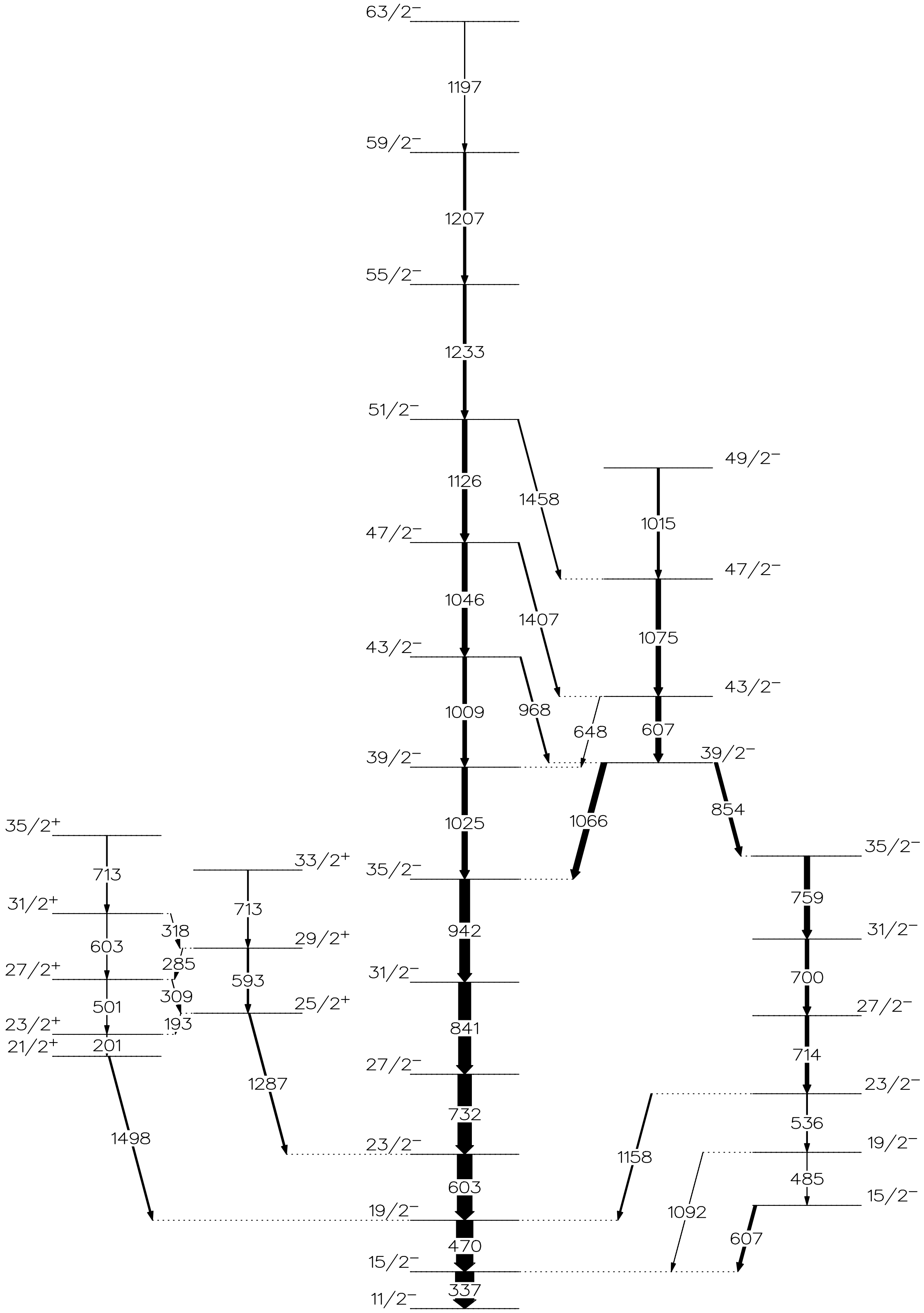

Figure 3: *Partial decay scheme of* ^{117}I.

equal ($R_{\text{DCO}} \equiv 1.0$), while, for an asymmetric geometry ($\theta_1 \neq \theta_2$), these intensities should also be equal ($R_{\text{DCO}} = 1.0$) for a cascade of two stretched $E2$ transitions (see Table 5).

7.1 Results for the individual geometries A–E

The coincidence data were first sorted into five separate angular-correlation matrices corresponding to the A–E geometries of the EUROGAM II spectrometer (see Table 3); The number of appropriate $\gamma - \gamma$ pairs incremented into these matrices were 160, 154, 148, 156, and 156 million pairs, respectively. Six of the yrast quadrupole transitions of ^{117}I (337, 470, 603, 841, 942, and 1015 keV) were used as gates, and the γ-rays in coincidence with these gates were projected out of each of these angular-correlation matrices onto both axes. Thus two 1-D spectra were obtained in each case. The extracted numbers of counts of the peaks (γ_1),

$$N_{\gamma_1\gamma} = \sum_j V_{\gamma_1\gamma_j}, \tag{20}$$

of some of the transitions in ^{117}I are listed in Table 7, together with experimental and theoretical DCO ratios. It can be seen that the experimental R_{DCO} ratios for the 470- and 942-keV transitions are very close to 1.00, justifying the assumption of equal detector efficiencies for the 30 coaxial detectors.

The 10 distinct intensities ($N_{\gamma_1\gamma}$, $N_{\gamma\gamma_1}$) shown in Table 7 for the known 1287-keV dipole transition of ^{117}I were used as input to the code GCORR, where they are compared to theoretical angular-correlation functions $W(\theta_1, \theta_2, \Delta\phi)$. In these calculations, the possible spins investigated for the 1287-keV transition were: (i) $J \to J$–2, (ii) $J \to J$–1, and (iii) $J \to J$; the results are shown in Fig. 4, which shows how χ^2 changes as a function of the mixing ratio δ (note that $J \to J$+1(2) transitions are equivalent to $J \to J$–1(2) transitions except that the sign of the multipole mixing ratio δ is reversed. Here we assume that there are no "uphill" transitions). The $J \to J$–2 option (dotted line) has a definite value of the mixing ratio inconsistent with zero (at the 99.9% confidence level). This option can be ruled out since it would imply octupole mixing, i.e. $E2/M3$ or $M2/E3$, which is highly

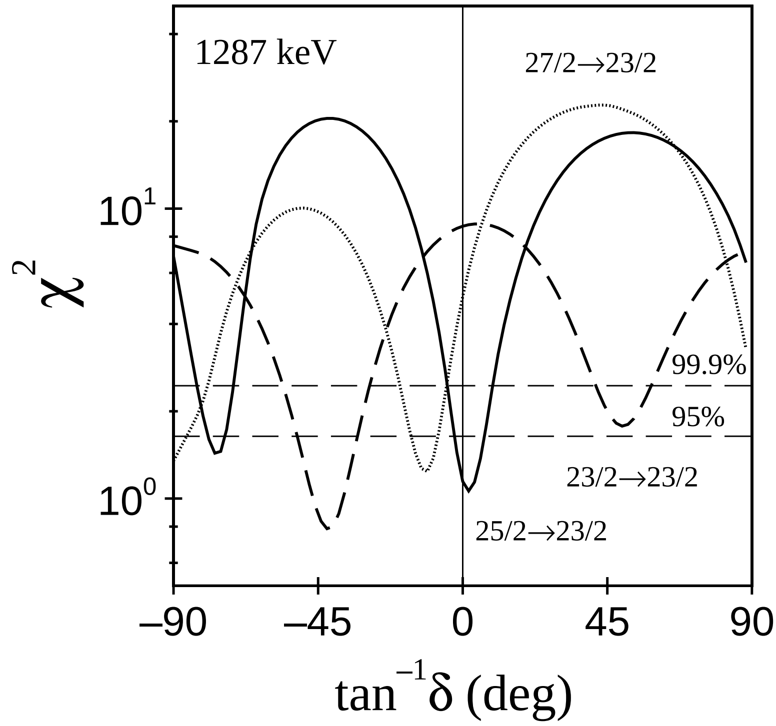

Figure 4: GCORR *analysis of the 1287-keV transition in* ^{117}I.

unlikely when considering the relative transition probabilities. The $J \rightarrow J$ option (dashed line) can also be rejected on similar physical grounds; the χ^2 minima near $\tan^{-1}\delta = \pm 45°$ correspond to multipole mixing ratios $\delta = \pm 1$, which implies (equation (2)) that the λ (dipole) and λ' (quadrupole) transitions have equal probability! The curve corresponding to the $J \rightarrow J$–1 option (solid line) is consistent with zero mixing, and hence the 1287-keV transition can be assigned as a pure stretched dipole. Since there is no mixing, an $E1$ assignment is preferred, although a measurement of the linear polarisation is required to distinguish between the possible electric and magnetic character.

In fact, the polarisation of this transition has been extracted from this data set, by considering the 24 four-element clover detectors of EUROGAM II as Compton polarimeters [11]. Two matrices were constructed from the coincidence data corresponding to single hits in any detector (coaxial or clover) on one axis against clover double-hit scattering events which are defined as either (i) "vertical" (perpendicular to the beam axis) or (ii)

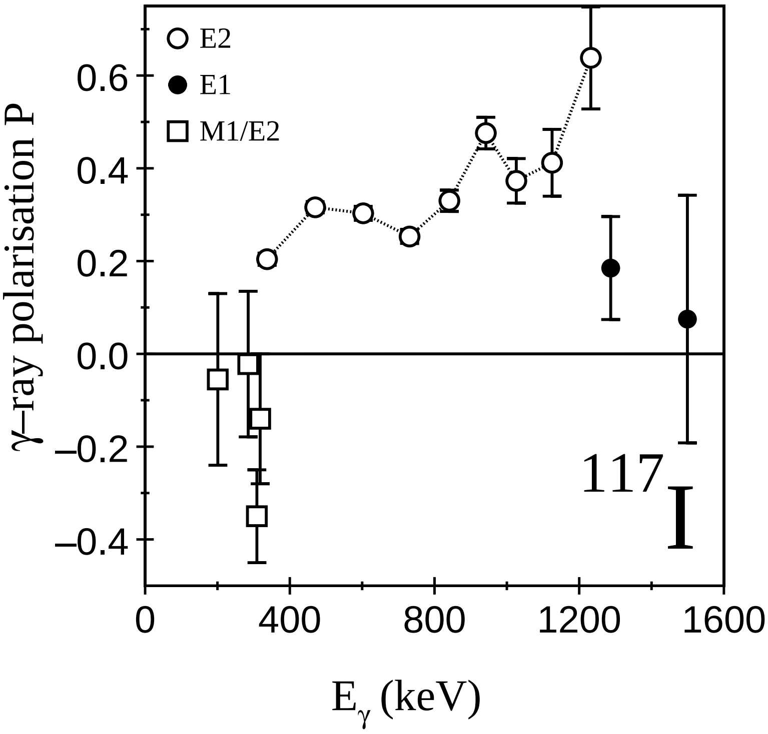

Figure 5: *Experimental linear polarisations of transitions in ^{117}I. The low-energy transitions are the $M1/E2$ 201-, 309-, 285-, and 318-keV dipoles. The high energy transitions are the $E1$ 1287- and 1498-keV linking transitions.*

"horizontal" (parallel to the beam axis). The number of vertical, N_V, and horizontal, N_H, scatters for a given γ-ray could be obtained by projecting out spectra gated by specific (^{116}Te) transitions on the single-hit axis. Assuming all 96 separate clover crystals have equal efficiencies, an experimental linear polarisation can be defined as

$$P = \frac{1}{Q}\frac{N_V - N_H}{N_V + N_H}, \tag{21}$$

where the polarisation sensitivity, Q, for the clover detectors is taken from Ref. [11]. The results are shown in Fig. 5, where the value obtained for the 1287-keV transition is positive and consistent with a stretched $E1$ dipole.

Similar arguments indicate that the 201- and 309-keV transitions in ^{117}I are stretched dipoles; fitting the data of Table 7 for these transitions, yields the χ^2 plot of Fig. 6. While the fits are not so good for these weak transitions, the results suggest nonzero delta val-

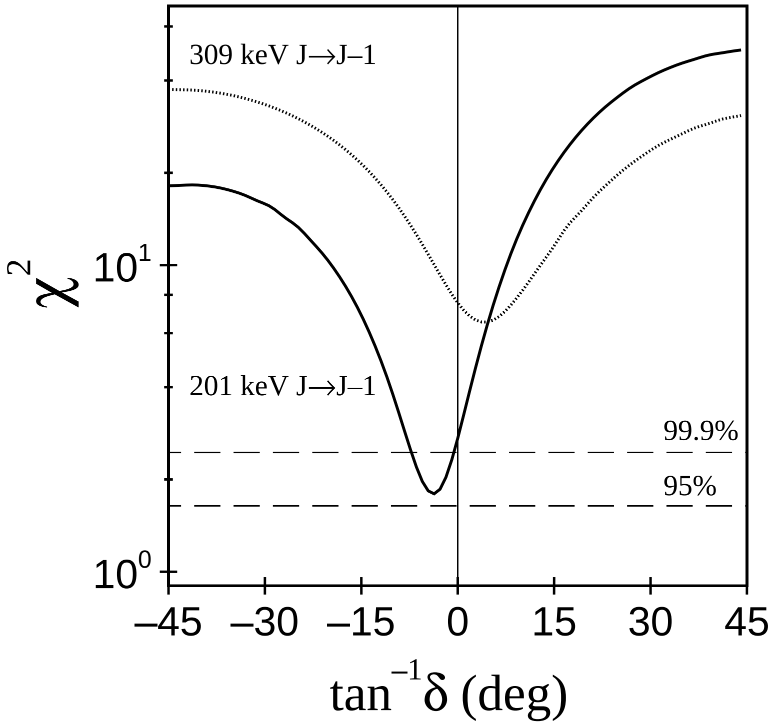

Figure 6: GCORR *analysis of the 201-keV and 309-keV dipoles in ^{117}I.*

ues, and hence mixed $M1/E2$ assignments. The (negative) measured linear polarisations, included in Fig. 5, corroborate these assignments. Furthermore, the 309-keV transition obviously links two signature partner bands (Fig. 3). Instead of using *ten* individual intensities as input to GCORR, *five* DCO ratios may be used instead. This removes some of the systematic errors, such as normalisation between the five angular-correlation matrices, and much better theoretical fits to the data can be obtained.

7.2 Results for the combined geometries A–E

Two angular-correlation matrices were constructed for the sum of all five geometries A–E. The first (ungated) matrix contained 774 million γ-ray pairs. The second (gated) matrix used six of the strongest transitions of ^{117}I [19] as gates before incrementing the matrix; 183 million γ-ray pairs were incremented into this latter matrix, which is more than the number of events extracted for the individual geometries. Table 8 shows numbers of counts extracted from these matrices, as discussed in the previous section, together with experimental and theoretical DCO ratios for the yrast quadrupole transitions in ^{117}I. Similarly, results for some dipole transitions in ^{117}I are listed in Table 9.

The increased statistics of the summed A–E geometries allow an R_{DCO} value to be obtained for the weak 1498-keV $E1$ transition [19]; this transition is too weak when considering the individual geometries. Similarly values can also be obtained for the 285- and 318-keV transitions (Fig. 3). The results of Tables 8 and 9 indicate that no sensitivity is lost in the discrimination of (stretched) quadrupole and dipole transitions when $\gamma - \gamma - \gamma$ events are considered. In the present analysis, using one γ-ray to gate the angular-correlation matrix decreased the number of counts by approximately a factor of five. The quality of spectra projected out of the matrix (effectively double-gated 1-D spectra) was, however, markedly improved. The low R_{DCO} value for the 201-keV $M1/E2$ transition is consistent with a negative multipole mixing ratio, while the higher values obtained for the intraband 309-, 285-, and 318-keV transitions are consistent with positive mixing ratios. Often, the determination of the SIGN of δ is sufficient to distinguish between possible theoretical band configurations.

The program XLII was used to investigate the combined-geometries A–E (ungated) matrix. The matrix was first background-subtracted using the BAC-PAC package. Peak volumes, $V_{\gamma_1\gamma_2}$, were then directly extracted for a specific pair of γ-rays. Results are shown in Table 10 for an $E2 \Leftrightarrow E2$ and $E1 \Leftrightarrow E2$ pair.

8 Conclusions

The sorting of EUROGAM II data into angular-correlation matrices, corresponding to different geometries (θ_1, θ_2, $\Delta\phi$) for specific detector pairs, has been outlined. Correlation intensities $I_{\gamma\gamma}(\theta_1, \theta_2, \Delta\phi)$ can be obtained from these matrices, and fitted to the theoretical $W(\theta_1, \theta_2, \Delta\phi)$ probabilities with the code GCORR [5], in order to assess proposed γ-ray multipolarities. Data from the EUROGAM II experiment EG43 are currently under analysis, using the methods outlined in this report, and preliminary results for ^{117}I have been discussed. This analysis has only considered the 30 coaxial detectors ($\theta = 22.4°, 46.4°$) of the EUROGAM II spectrometer. Dave Cullen is presently investigating DCO analysis including the clover detectors ($\theta = 75.5°$) for a data set on ^{172}Hf.

A similar correlation analysis may be applied to the 110-detector GAMMASPHERE spectrometer, for which there are 204 separate geometries[10], while the complex angular layout of EUROBALL III may require further thought!

9 Acknowledgments

The programs COMBIN, CORR_EFF, and GCORR were acquired from Peter Ekström at the University of Lund, Sweden, via the WorldWideWeb (http://www.fysik.lu.se/nucleardata/). Preprints describing these programs are also available from this site. The program CORREL was acquired from Risø via Manchester. The X-windows version (XLII) of the program 42 [17], together with the BAC-PAC package, were installed on the Liverpool SUNS by Mats Bergström; manuals are available from ESP. The fortran sorting code FAZSORT was originally developed by Paul Fallon and Con Beausang.

[10]all 204 geometries are listed in the file /home/user/esp/DCO/combin/gsdets.out

References

[1] P.J. Twin and J.C. Willmott, Nucl. Phys. **78**, 177 (1966).

[2] B. Grosswendt and E. Waibel, Z. Phys. **A277**, 375 (1976).

[3] M.A. van Driel, G.A.P. Engelbertink, H.H. Eggenhuisen, L.P. Ekström, and J.A.J. Hermans, Phys. Lett. **B59**, 336 (1975).

[4] A. Krämer-Flecken, T. Morek, R.M. Lieder, W. Gast, G. Hebbinghaus, H.M. Jäger, and W. Urban, Nucl. Instrum. and Methods **A275**, 333 (1989).

[5] L.P. Ekström and A. Nordlund, Nucl. Instrum. and Methods **A313**, 421 (1992).

[6] P.J. Nolan, F.A. Beck, and D.B. Fossan, Annu. Rev. Nucl. Part. Sci. **45**, 561 (1994).

[7] K.S. Krane, R.M. Steffen, and R.M. Wheeler, Nucl. Data Tables **A11**, 351 (1973).

[8] T. Yamazaki, Nucl. Data **A3**, 1 (1967).

[9] H.J. Rose and D.M. Brink, Revs. Mod. Phys. **39**, 306 (1967).

[10] C.W. Beausang, D. Prévost, M.H. Bergstrom, G. deFrance, B. Haas, J.C. Lisle, Ch. Theisen, J. Timár, P.J. Twin, and J.N. Wilson, Nucl. Instrum. and Methods **A364**, 560 (1995).

[11] P.M. Jones, L. Wei, F.A. Beck, P.A. Butler, T. Byrski, G. Duchêne, G. deFrance, F. Hannachi, G.D. Jones, and B. Kharraja, Nucl. Instrum. and Methods **A362**, 556 (1995).

[12] A.T. Semple, Thesis, University of Liverpool (1995).

[13] M.A. Bentley et al., J. Phys. G **17**, 481 (1991).

[14] D.M. Cullen, Thesis, University of Liverpool (1991).

[15] E.S. Paul, D.B. Fossan, K. Hauschild, I.M. Hibbert, H. Schnare, J.M. Sears, I. Thorslund, R. Wadsworth, A.N. Wilson, and J.N. Wilson, Phys. Rev. C **51**, R2857 (1995).

[16] D.C. Radford, Nucl. Instrum. and Methods **A361**, 297 (1995).

[17] M. Bergström and P. Ekström, Nucl. Instrum. and Methods **A301**, 132 (1991).

[18] G. Palameta and J. Waddington, Nucl. Instrum. and Methods **A234**, 476 (1985).

[19] M.P. Waring, D.B. Fossan, J.R. Hughes, D.R. LaFosse, Y. Liang, R. Ma, P. Vaska, S.A. Forbes, E.S. Paul, R.M. Clark, and R. Wadsworth, Phys. Rev. C **48**, 2629 (1993).

Tables

Table 1. Angular layout of the EUROGAM II spectrometer. Large-volume coaxial detectors occupy positions 1–30 at forward/backward angles, while segmented clover detectors occupy positions 31–54 near $\theta \sim 90°$.

Array position	θ (deg) [a]	ϕ (deg) [b]
1	157.6	0.0
2	157.6	72.0
3	157.6	144.0
4	157.6	216.0
5	157.6	288.0
6	133.6	18.0
7	133.6	54.0
8	133.6	90.0
9	133.6	126.0
10	133.6	162.0
11	133.6	198.0
12	133.6	234.0
13	133.6	270.0
14	133.6	306.0
15	133.6	342.0
16	46.4	18.0
17	46.4	54.0
18	46.4	90.0
19	46.4	126.0
20	46.4	162.0
21	46.4	198.0
22	46.4	234.0
23	46.4	270.0
24	46.4	306.0
25	46.4	342.0
26	22.4	0.0
27	22.4	72.0

Table 1. Continued.

Array position	θ (deg) [a]	ϕ (deg) [b]
28	22.4	144.0
29	22.4	216.0
30	22.4	288.0
31	104.5	15.0
32	75.5	15.0
33	104.5	45.0
34	75.5	45.0
35	104.5	75.0
36	75.5	75.0
37	104.5	105.0
38	75.5	105.0
39	104.5	135.0
40	75.5	135.0
41	104.5	165.0
42	75.5	165.0
43	104.5	195.0
44	75.5	195.0
45	104.5	225.0
46	75.5	225.0
47	104.5	255.0
48	75.5	255.0
49	104.5	285.0
50	75.5	285.0
51	104.5	315.0
52	75.5	315.0
53	104.5	345.0
54	75.5	345.0

[a] The angle $\theta = 0°$ defines the beam direction (z-axis).

[b] The angle $\phi = 0°$ is arbitrarily defined as directly up, and ϕ increases clockwise when viewing the array from a position upstream.

Table 2. Number of specific geometries for the EUROGAM II spectrometer, and their number of two-detector combinations, calculated with the code COMBIN [5]. The total number of geometries is 83 ($\sum N_g$), while the total number of two-detector pairs is 1431 ($\sum N_g N_c$).

No. geometries N_g	No. combinations N_c	$N_g \times N_c$
5	48	240
9	40	360
1	24	24
1	20	20
30	16	480
1	12	12
5	10	50
30	8	240
1	5	5
$\sum = 83$		$\sum = 1431$

Table 3. Number of two-detector combinations, from the possible 83 geometries of the EUROGAM II spectrometer, that contain 40 or more combinations.

Geometry label [a]	θ_1 (deg)	θ_2 (deg)	$\Delta\phi$ (deg)	No. detector combinations
A	22.4	46.4	18.0	40
B	22.4	46.4	54.0	40
C	22.4	46.4	90.0	40
D	22.4	46.4	126.0	40
E	22.4	46.4	162.0	40
F	46.4	46.4	36.0	40
G	46.4	46.4	72.0	40
H	46.4	46.4	108.0	40
I	46.4	46.4	144.0	40
J	75.5	75.5	30.0	48
K	75.5	75.5	60.0	48
L	75.5	75.5	90.0	48
M	75.5	75.5	120.0	48
N	75.5	75.5	150.0	48

[a] Note that the five geometries A–E are asymmetric ($\theta_1 \neq \theta_2$), while the nine geometries F–N are symmetric ($\theta_1 = \theta_2$). Geometries A–I contain only coaxial detectors, while geometries J–N contain only clover detectors.

Table 4. The 40 coaxial detector pairs, at array positions (x,y) (see Table 1), that constitute geometry A ($\theta_1 = 22.4°$, $\theta_2 = 46.4°$, $\Delta\phi = 18.0°$) of the EUROGAM II spectrometer.

(1,6)	(1,15)	(1,20)	(1,21)	(2,7)	(2,8)	(2,22)	(2,23)
(3,9)	(3,10)	(3,24)	(3,25)	(4,11)	(4,12)	(4,16)	(4,17)
(5,13)	(5,14)	(5,18)	(5,19)	(29,6)	(29,7)	(30,8)	(30,9)
(26,10)	(26,11)	(27,12)	(27,13)	(28,14)	(28,15)	(26,16)	(27,17)
(27,18)	(28,19)	(28,20)	(29,21)	(29,22)	(30,23)	(30,24)	(26,25)

Table 5. Values of the angular-correlation function $W(\theta_1,\ \theta_2,\ \Delta\phi)$ calculated with the program CORREL for the asymmetric A–E geometries of the EUROGAM II spectrometer. The $R_{\rm DCO}$ ratios $(W(\theta_1,\ \theta_2,\ \Delta\phi)/\ W(\theta_2,\ \theta_1,\ \Delta\phi))$ are also given for pure stretched $E2 \Leftrightarrow E2$ (quadrupole $\Leftrightarrow$ quadrupole) and $E1 \Leftrightarrow E2$ (dipole $\Leftrightarrow$ quadrupole) sequences.

Spin sequence	$W(22.4°, 46.4°, 18°)$	$W(46.4°, 22.4°, 18°)$	$R_{\rm DCO}$ $[E2 \Leftrightarrow E2]$	$R_{\rm DCO}$ $[E1 \Leftrightarrow E2]$
$12 \xrightarrow{E2} 10 \xrightarrow{E2} 8$	1.398	1.398	1.000	
$11 \xrightarrow{E1} 10 \xrightarrow{E2} 8$	0.921	1.193		0.772
	$W(22.4°, 46.4°, 54°)$	$W(46.4°, 22.4°, 54°)$		
$12 \xrightarrow{E2} 10 \xrightarrow{E2} 8$	1.412	1.412	1.000	
$11 \xrightarrow{E1} 10 \xrightarrow{E2} 8$	0.921	1.187		0.776
	$W(22.4°, 46.4°, 90°)$	$W(46.4°, 22.4°, 90°)$		
$12 \xrightarrow{E2} 10 \xrightarrow{E2} 8$	1.432	1.432	1.000	
$11 \xrightarrow{E1} 10 \xrightarrow{E2} 8$	0.917	1.174		0.781
	$W(22.4°, 46.4°, 126°)$	$W(46.4°, 22.4°, 126°)$		
$12 \xrightarrow{E2} 10 \xrightarrow{E2} 8$	1.449	1.449	1.000	
$11 \xrightarrow{E1} 10 \xrightarrow{E2} 8$	0.906	1.160		0.781
	$W(22.4°, 46.4°, 162°)$	$W(46.4°, 22.4°, 162°)$		
$12 \xrightarrow{E2} 10 \xrightarrow{E2} 8$	1.458	1.458	1.000	
$11 \xrightarrow{E1} 10 \xrightarrow{E2} 8$	0.896	1.150		0.779

Table 6. Values of the angular-correlation function $W(\theta_1,\ \theta_2,\ \Delta\phi)$ calculated with the program CORREL for the symmetric F–I geometries of the EUROGAM II spectrometer. Since $\theta_1 = \theta_2$, the R_{DCO} ratio carries no information ($\equiv 1.0$ always).

Spin sequence	$W(46.4°, 46.4°, 36°)$
$12 \xrightarrow{E2} 10 \xrightarrow{E2} 8$	1.289
$11 \xrightarrow{E1} 10 \xrightarrow{E2} 8$	1.094
	$W(46.4°, 46.4°, 72°)$
$12 \xrightarrow{E2} 10 \xrightarrow{E2} 8$	1.292
$11 \xrightarrow{E1} 10 \xrightarrow{E2} 8$	1.104
	$W(46.4°, 46.4°, 108°)$
$12 \xrightarrow{E2} 10 \xrightarrow{E2} 8$	1.310
$11 \xrightarrow{E1} 10 \xrightarrow{E2} 8$	1.092
	$W(46.4°, 46.4°, 144°)$
$12 \xrightarrow{E2} 10 \xrightarrow{E2} 8$	1.332
$11 \xrightarrow{E1} 10 \xrightarrow{E2} 8$	1.064

Table 7. Experimental numbers of counts and R_{DCO} ratios for transitions in ^{117}I, assuming the coaxial detectors all have equal intensities.

E_{γ_1} (keV)	$I_i^{\pi_i} \rightarrow I_f^{\pi_f}$	Geometry	$N_{\gamma_1\gamma}$	$N_{\gamma\gamma_1}$	R_{DCO}	$R_{\text{DCO},th}$ [a]
470	$\frac{19}{2}^- \rightarrow \frac{15}{2}^-$	A	38938(225)	40616(230)	0.94(01)	1.00
		B	40960(225)	40441(235)	1.01(01)	
		C	39085(220)	39376(220)	0.99(01)	
		D	37520(220)	39571(220)	0.98(01)	
		E	41321(225)	42068(220)	0.98(01)	
942	$\frac{35}{2}^- \rightarrow \frac{31}{2}^-$	A	14814(170)	14447(170)	1.03(01)	1.00
		B	15419(170)	14268(175)	1.08(02)	
		C	13654(160)	12911(165)	1.06(02)	
		D	13376(160)	13068(165)	1.02(02)	
		E	14117(160)	14271(165)	0.99(01)	
1287	$\frac{25}{2}^+ \rightarrow \frac{23}{2}^-$	A	1510(96)	1893(100)	0.80(06)	0.78
		B	1416(85)	1821(120)	0.78(07)	
		C	1372(90)	1744(95)	0.79(08)	
		D	1305(95)	1585(95)	0.82(09)	
		E	1255(85)	1505(95)	0.83(09)	
201	$\frac{23}{2}^+ \rightarrow \frac{21}{2}^+$	A	1266(75)	1932(75)	0.66(04)	0.78 [b]
		B	1476(80)	2125(85)	0.69(05)	
		C	1662(75)	1993(80)	0.84(07)	
		D	1443(75)	1799(85)	0.80(07)	
		E	1421(70)	2078(85)	0.68(05)	
309	$\frac{27}{2}^+ \rightarrow \frac{25}{2}^+$	A	2314(95)	2534(95)	0.91(05)	0.78 [b]
		B	1876(95)	2365(100)	0.79(05)	
		C	2010(85)	2622(90)	0.77(05)	
		D	1952(80)	2511(90)	0.78(05)	
		E	1878(80)	2694(90)	0.70(05)	

[a] Theoretical R_{DCO} (see Table 5).

[b] Assuming $\delta_{E2/M1} = 0$.

Table 8. Experimental numbers of counts and R_{DCO} ratios for the yrast quadrupole transitions in ^{117}I (see Fig. 3). Theoretically, $R_{\mathrm{DCO}} = 1.00$ (see Table 5).

E_{γ_1} (keV)	$I_i^{\pi_i} \rightarrow I_f^{\pi_f}$	$N_{\gamma_1\gamma}$	$N_{\gamma\gamma_1}$	R_{DCO} [a]	R_{DCO} [b]
337	$\frac{15}{2}^- \rightarrow \frac{11}{2}^-$	211681(510)	230912(570)	0.92(01)	
		83679(320)	87469(330)		0.96(01)
470	$\frac{19}{2}^- \rightarrow \frac{15}{2}^-$	207231(520)	203164(532)	1.02(01)	
		81340(320)	80371(320)		1.01(01)
603	$\frac{23}{2}^- \rightarrow \frac{19}{2}^-$	161308(470)	159083(480)	1.01(01)	
		74198(310)	73390(315)		1.01(01)
732	$\frac{27}{2}^- \rightarrow \frac{23}{2}^-$	142682(470)	149873(480)	0.95(01)	
		71376(305)	71745(330)		0.99(01)
841	$\frac{31}{2}^- \rightarrow \frac{27}{2}^-$	91450(380)	92001(400)	0.99(01)	
		50407(275)	49896(290)		1.01(01)
942	$\frac{35}{2}^- \rightarrow \frac{31}{2}^-$	72995(375)	68429(400)	1.07(01)	
		41494(260)	39913(270)		1.04(01)
1025	$\frac{39}{2}^- \rightarrow \frac{35}{2}^-$	42160(330)	40663(330)	1.04(01)	
		20609(205)	20385(210)		1.01(02)
1009	$\frac{43}{2}^- \rightarrow \frac{39}{2}^-$	20408(285)	20681(305)	0.99(02)	
		13571(185)	12475(190)		1.09(03)
1046	$\frac{47}{2}^- \rightarrow \frac{43}{2}^-$	24101(275)	23954(305)	1.01(02)	
		14231(180)	13673(195)		1.04(03)
1126	$\frac{51}{2}^- \rightarrow \frac{47}{2}^-$	23040(285)	22519(282)	1.02(02)	
		13347(180)	13660(190)		0.98(03)
1233	$\frac{55}{2}^- \rightarrow \frac{51}{2}^-$	14204(250)	14511(250)	0.98(03)	
		7080(160)	7220(175)		0.98(04)
1207	$\frac{59}{2}^- \rightarrow \frac{55}{2}^-$	8330(235)	8052(220)	1.03(04)	
		3849(145)	3490(150)		1.10(07)

[a] Composite R_{DCO} for the A–E geometries (ungated matrix).

[a] Composite R_{DCO} for the A–E geometries (gated matrix).

Table 9. Experimental numbers of counts and R_{DCO} ratios for some dipole transitions in ^{117}I (see Fig. 3). Theoretically, $R_{\text{DCO}} = 0.78$ (see Table 5), assuming $\delta = 0$.

E_{γ_1} (keV)	$I_i^{\pi_i} \rightarrow I_f^{\pi_f}$	$N_{\gamma_1\gamma}$	$N_{\gamma\gamma_1}$	R_{DCO} [a]	R_{DCO} [b]
1287	$\frac{25}{2}^+ \rightarrow \frac{23}{2}^-$	8040(225)	10180(275)	0.79(03)	
$E1$		2146(120)	2704(150)		0.79(07)
1498	$\frac{21}{2}^+ \rightarrow \frac{19}{2}^-$	2410(155)	3042(170)	0.79(07)	
$E1$		—	—		—
201	$\frac{23}{2}^+ \rightarrow \frac{21}{2}^+$	7638(180)	11175(210)	0.68(02)	
$M1/E2$		2049(100)	2824(120)		0.73(05)
309	$\frac{27}{2}^+ \rightarrow \frac{25}{2}^+$	9890(220)	12399(250)	0.80(03)	
$M1/E2$		2447(111)	2838(125)		0.86(06)
285	$\frac{29}{2}^+ \rightarrow \frac{27}{2}^+$	8167(195)	9537(195)	0.86(03)	
$M1/E2$		2059(110)	2331(110)		0.88(07)
318	$\frac{31}{2}^+ \rightarrow \frac{29}{2}^+$	4553(165)	5582(185)	0.82(04)	
$M1/E2$		1589(100)	1850(115)		0.86(08)

[a] Composite R_{DCO} for the A–E geometries (ungated matrix).

[a] Composite R_{DCO} for the A–E geometries (gated matrix).

Table 10. Peak volumes obtained directly from the ungated, combined-geometries A–E matrix, using the program XLII.

	$\gamma_1 - \gamma_2$	$V_{\gamma_1\gamma_2}$	$V_{\gamma_2\gamma_1}$	R_{DCO}
$E2 \Leftrightarrow E2$	470–337	116613(340)	110473(335)	1.06(05)
$E1 \Leftrightarrow E2$	1287–337	4622(70)	5494(75)	0.85(03)